# Investigation of de novo mutations in a schizophrenia case-parent trio by induced pluripotent stem cell based in vitro disease-modeling: Convergence of schizophrenia and autism-related cellular phenotypes

**Edit Hathy**
Semmelweis Egyetem Doktori Iskola
**Nóra Varga**
Research Centre for Natural Sciences
**Zsuzsa Erdei**
Research Centre for Natural Sciences
**Eszter Szabó**
Research Centre for Natural Sciences
**Csongor Tordai**
Semmelweis University
**Boróka Czehlár**
Semmelweis University
**Máté Baradits**
Semmelweis University
**Bálint Jezsó**
Research Centre for Natural Sciences
**Júlia Koller**
Semmelweis University
**László Nagy**
University of Debrecen
**Mária Judit Molnár**
Semmelweis University
**Zsófia Nemoda**
Semmelweis University
**László Homolya**
Research Centre for Natural Sciences
**Ágota Apáti**
Research Centre for Natural Sciences

**János M Réthelyi** ( rethelyi.janos@med.semmelweis-univ.hu )
Semmelweis University https://orcid.org/0000-0002-3641-012X

**Research**

**Keywords:** Schizophrenia, Autism, DNM, KHSRP, LRRC7, iPSC, Disease-modeling, RNASeq, Mitochondrial function

**Posted Date:** January 13th, 2020

**DOI:** https://doi.org/10.21203/rs.2.20699/v1

# Abstract

Background: De novo mutations (DNMs) have been implicated in the etiology of schizophrenia, a chronic debilitating psychiatric disorder characterized by hallucinations, delusions, cognitive dysfunction and poor community functioning. Several DNMs have been shown by examining schizophrenia cases and their unaffected parents, however in most cases the biological significance of these mutations remains elusive. To overcome this limitation we have developed an approach of using somatic cell reprogramming to generate induced pluripotent stem cell (iPSC) lines from each member of a schizophrenia case-parent trio, in order to investigate the effects of DNMs in cellular progenies of interest, particularly in dentate gyrus neuronal progenitors.

Methods: We identified a male schizophrenia patient characterized by early disease onset and negative symptoms, who is a carrier of 3 non-synonymous DNMs in genes LRRC7, KHSRP, and KIR2DL1. iPSC lines were generated from his and his parents' peripheral blood mononuclear cells using Sendai virus-based reprogramming. After characterization the iPSCs were differentiated into neuronal progenitor cells (NPCs) and hippocampal dentate gyrus granule cells for the investigation of various cellular phenotypes. We used RNASeq to investigate and transcriptomic differences, calcium (Ca 2+ ) imaging, cell proliferation, migration, oxidative stress, and mitochondrial assays to characterize the investigated NPC lines.

Results: NPCs derived from the schizophrenia patient exhibited transcriptomic differences related to Wnt-signaling, axonal guidance and synapse formation, and decreased Ca 2+ reactivity to glutamate. Moreover we could observe increased cellular proliferation and migration, accelerated neurite outgrowth rates, and alterations in mitochondrial quantity and morphology.

Conclusions: The approach of reprograming case-parent trios represents a possibility of investigating disease-causing mutations and comparing cell lines with reduced variation in genetic background. Our results are indicative of an overlap between schizophrenia and autism-related phenotypes in the investigated family.


# Background

Schizophrenia is a chronic, debilitating psychiatric disorder characterized by hallucinations, delusions, social withdrawal, cognitive dysfunction and decreased community functioning. Despite considerable development in pharmacological and psychosocial therapeutic possibilities, one third of patients does not respond to existing treatment interventions, and demonstrates a poor outcome (1, 2). The molecular and neurobiological processes underlying this disorder are poorly understood, therefore, based on the unmet medical need and our limited knowledge of disease pathways, new research approaches are needed to improve our insight of the etiology of schizophrenia.

Induced pluripotent stem cell (iPSC) based disease modeling represents a new avenue of research in the investigation of neuropsychiatric disorders that has been successfully used to study molecular disease

pathways in this disease group. Briefly, this approach takes advantage of somatic cell reprogramming, which results in iPSC lines that capture genetic variants carried by diseased individuals. After reprogramming, the effects of these putative disease-causing variants can be investigated on various molecular and functional phenotypes in neuronal cell types of interest, by using targeted differentiation protocols (3–5).

Previous efforts to elucidate the genetic background of schizophrenia and autism have identified both common and rare variants that show association with disease status or various disease-related phenotypes (6). Interestingly, both common and rare disease causing genetic variants, i.e. single nucleotide polymorphisms (SNPs) and single nucleotide variants (SNVs) or copy number variants (CNVs), respectively, show a considerably degree of overlap between schizophrenia and other psychiatric disorders, including autism spectrum disorder (7–11). De novo mutations (DNMs) are a subclass of SNVs, in cases where the mutations appear unprecedentedly, de novo in a given generation, and represent a unique source of genetic variation that plays a role both in autism and schizophrenia. Genetic research focusing on DNMs highlights the importance of variants in evolutionarily conserved, mutation-intolerant genes that perturb downstream essential molecular pathways in neurons (12).

The effects of schizophrenia-associated genetic variants have been investigated previously in iPSCs both directly and indirectly, i.e. by using cell lines with known genetic variants (13), or studying cell lines derived from sporadic schizophrenia cases, without established genetic alterations (14). In the latter studies the patient-derived cell lines were considered and investigated based on the fact that they originate from patients diagnosed with schizophrenia, i.e. their genome carries potential risk variants, without knowing which variants are present in that patient. The field of iPSC-based disease modeling studies was founded by the seminal paper of Brennand et al. in 2011 that has been followed by several studies looking at different aspects of schizophrenia-related in vitro phenotypes. Reviews comparing these studies have been looking at overlapping findings between these results, and identified glutamatergic synaptic dysfunction, Wnt-signaling and increased oxidative stress as potentially significant in vitro phenotypes for schizophrenia (15, 16). Recently CRISPR genome editing was exploited in iPSCs to generate isogenic cell lines that are genetically identical except for a known schizophrenia risk variant. This study was able to show that a single SNP can give rise to differential neuronal phenotypes and establish expression quantitative trait loci. Harnessing genome editing technologies to investigate clinically established risk variants will foreseeably play an important role in the field.

In order to investigate the biological functions of schizophrenia DNMs in an in vitro cellular context one possible approach is the investigation of isogenic cell lines after introduction or correction of a DNM by genome editing. This approach has been used for schizophrenia in one previous study, however the focus were common schizophrenia risk variants (17, 18). Another potential way of investigation is to use case-parent trios, and generate iPSC lines from the proband and both parents. This approach simulates both familial risk and the effects of the de novo mutation. Recently a family enriched for autism spectrum disorder has been investigated using iPSC-based disease modeling (19).

Based on our previous exome-sequencing results and bioinformatics analyses, we focused on downstream effects of 3 genes, LRRC7, KHSRP, KIR2DL1, in which DNMs were identified in the schizophrenia patient. K-homology type splicing regulatory protein (KHSRP) is a RNA-binding protein that modulates RNA life and gene expression at different levels, including mRNA decay, miRNA biogenesis, and by its interaction with lncRNAs (20). It is localized to the nucleus and cytoplasmic granules. Biological significance of this gene has been shown in cell fate determination, immune response, neuronal differentiation and neurite outgrowth. Based on its diverse roles as an RNA-binding protein in neurons, it has been suggested to play an etiologic role in several neuropsychiatric disorders (21). KHSRP has also been identified as a potential schizophrenia biomarker in a study based on transcriptomic differences in circulating white blood cells (22).

Leucine Rich Repeat Containing 7 (LRRC7) encodes densin-180, a postsynaptic density protein in glutamatergic synapses. In an LRRC7 KO animal model the lack of this protein resulted in decreased dendritic spine number and altered behavioral phenotypes (23). LRRC7 is also associated with emotional dysregulation and autistic traits, mutant mice in a KO model had inappropriate juvenile aggressive behavior and significant anxiety-like behavior and social dysfunction in adulthood. Killer cell immunoglobulin-like receptor 2DL1 (KIR2DL1) encodes killer cell immunoglobulin-like receptors that are transmembrane glycoproteins expressed by natural killer cells and certain T cells, and plays a role in regulating immune responses (24). Due to the gene's tissue-specific expression patterns, this DNM was not expected to play any role in neuronal differentiation processes or neuronal functions, and therefore, not taken forward for characterization in this study.

In summary, we have investigated the biological effects of DNMs identified in a schizophrenia patient using iPSC-based disease-modeling applied to all members of a case-parent trio. After generation of iPSCs and neuronal differentiation into hippocampal dentate gyrus granule cells, we sought transcriptomic alterations and phenotypic differences related to schizophrenia according to previous studies. We were able to uncover marked transcriptomic differences and subtle physiological alterations in the proband-derived neuronal progenitor cells related to neuronal progenitor proliferation and migration, mitochondrial function, and calcium-signaling. The rationale of this approach of using a case-parent trio as a model-system was to contrast cell lines with known genetic alterations, but otherwise limited differences in genetic background. Based on mutation prediction tools we hypothesized transcriptomic alterations related to previously known biological functions of KHSRP, however other potential changes due to the other DNMs couldn't be ruled out either, therefore we investigated changes related to LRRC7 function as well.

# Methods

### Subject selection and characterization, identification of de novo mutations

We used cell lines derived from 4 human subjects (SZ-HU-PROB, SZ-HU-MO, SZ-HU-FA, and 62F), a schizophrenia patient and his parents, i.e. a case-parent trio, and an unrelated healthy control (Table 1 and Figure 1a) for all experiments. (The patient's two siblings, an unaffected brother and a sister diagnosed with bipolar affective disorder, were not included neither in the genetic analysis, nor the subsequent cell reprogramming.) The patient diagnosed with schizophrenia was selected from 16 similar trios, based on de novo mutations (DNMs) identified by exome sequencing, i.e. single nucleotide variants found in the patient, but not in the parents. The ExomeSeq analysis was carried out after 100 bp paired ended sequencing that was run on the Illumina HiScan(TM)SQ platform and resulted in 50 M reads on average per sample. Results were analyzed by a standard bioinformatics pipeline. The identified DNMs were validated by Sanger sequencing. The schizophrenia patient (SZ-HU-PROB) is a carrier of 3 missense DNMs in genes KHSRP (19:6416869C>A), LRRC7 (1:70505093G>A), and KIR2DL1 (19:55286658A>T). Of these, SIFT mutation algorithm predicts the KHSRP mutation as deleterious (Figures 1b and Table 2). None of these DNMs have been reported previously to the ClinVar database (25).

**Table 1.** Demographic and clinical data of the investigated case-parent trio, the extended family, and the unrelated healthy control individual.

| Subject | Sex | Age | Medical history | Reprogramming method | Code |
|---|---|---|---|---|---|
| **Father** | M | 59 | No psychiatric treatment or other major somatic disorder. | Sendai virus reprogramming from blood PBMCs. | IPSC-SZ-HU-FA |
| **Mother** | F | 55 | No psychiatric treatment or other major somatic disorder. | Sendai virus reprogramming from blood PBMCs. | IPSC-SZ-HU-MO |
| **Proband (son)** | M | 24 | Diagnosed with schizophrenia at the age of 17. During the past 10 years had 7 hospitalizations, receives clozapine treatment. Predominantly negative symptoms, as measured by PANSS. | Sendai virus reprogramming from blood PBMCs. | IPSC-SZ-HU-PROB |
| **Unaffected older sibling** | M | 28 | No psychiatric treatment or other major somatic disorder. | - | - |
| **Younger sibling** | F | 21 | Diagnosed with bipolar affective disorder at age of 18 after suicidal attempt. Receives lithium and olanzapine treatment. | - | - |
| **Unrelated healthy control** | M | 35 | No psychiatric treatment or other major somatic disorder. | Sendai virus reprogramming from skin fibroblasts. | IPSC-62F |

**Table 2.** Description of the identified DNMs in the schizophrenia proband.

| Genomic position | 1:70505093G>A | 19:6416869C>A | 19:55286658A>T |
|---|---|---|---|
| Gene | LRRC7 | KHSRP | KIR2DL1 |
| Variation type | missense | missense | missense |
| Amino acid change | Val1158Ile | Gly403Cys | Thr138Ser |
| Conservation of nucleotide | weak | high | not conserved |
| Conservation of amino acid | high | moderate | weak |
| SIFT | tolerated (score: 0.37, median: 4.32) | deleterious (score: 0.03, median: 3.54) | tolerated (score: 0.73, median: 3.01) |
| Mutation taster | polymorphism (p-value: 0.999) | disease causing (p-value: 0.996) | polymorphism (p-value: 1) |

## Generation and characterization of iPSC lines

Blood samples were obtained from trio members after written informed consent. The reprogramming and the study were approved by the Human Reproduction Committee of the Hungarian Health Science Council (ETT HRB). Blood was collected directly to cell preparation tubes with sodium heparin (BD Vacutainer CPT) to isolate peripheral mononuclear cells (PBMCs) from all samples. PBMCs were cultured for 4 days with daily medium changes at a density of $5 \times 10^5$ cells/ml in StemPro®-34 (Thermo Fisher) hematopoietic medium supplemented with 2 mM L-Glutamine and cytokines at the following final concentrations (SCF 100 ng/mL, FLT-3 100 ng/mL, IL-3 20 ng/mL, IL-6 20 ng/mL, all from Peprotech). On day 4, PBMCs were transduced with Sendai virus (Fusaki et al., 2009) particles (Thermo Fisher Cytotune 2.0) carrying KOS (hKlf4, hOct3/4, hSox2), hc-Myc, and hKlf4 at MOIs of 5, 5 and 3, respectively. After addition of the virus particles, samples were centrifuged in a 12 well plate for 90 minutes at 2250 rpm and incubated at 37°C overnight. After changing the medium, the cells were maintained for additional 2 days, then transferred to culturing dishes previously seeded with mouse embryonic fibroblasts (MEFs)

and cultured in StemPro®-34 medium without cytokines. Six days after transduction, the culturing medium over the cells was gradually changed to HUES medium (KO-DMEM, supplemented with 15% KO Serum Replacement (Thermo Fisher), 100 mM glutamine, 1% nonessential amino acids, 0.1 mM β-Mercaptoethanol and 4 ng/ml recombinant human basic fibroblast growth factor, bFGF).

14-18 days after transduction, individual iPSC colonies emerging were mechanically isolated and transferred to MEFs to generate clones. To ensure virus clearance and monitor stability, the clones were repeatedly passaged and expanded up to p10 using trypsin. Heat treatment at 38.5°C was used between passage p4-p8 to take advantage of the heat sensitivity of virus particles. iPSC 62F was generated from fibroblasts using Sendai virus reprogramming, independently from the other trio iPSC lines.

The pluripotent state and spontaneous differentiation capacity of iPSCs were tested by real-time quantitative PCR and ICC (Figure 1 c,d) as described previously (26). The investigated KHSRP and LRRC7 DNMs were cross-checked in the iPSCs with Sanger sequencing (Figure 1e).

## Cell culturing and neuronal differentiation

Neural progenitor cells (NPCs) were differentiated from iPSC lines SZ-HU-PROB, SZ-HU-MO, SZ-HU-FA, and 62F (unrelated healthy control) as described previously (27, 28). Briefly, before starting differentiation, iPSC cells were transferred to Matrigel (Corning, New York, USA) coated plates in mTeSR medium (Stemcell Technologies, Vancouver, Canada) and were cultured to high density. On day 1 the cells were detached with collagenase (Thermo Fisher Scientific, Massachusetts, USA) and transferred to ultra-low attachment plates (Nalgene Nunc International, New York, USA). After embryoid body (EB) formation, the medium was changed to DMEM/F-12, GlutaMAX™ (Thermo Fisher Scientific, Massachusetts, USA) medium supplemented with N2/B27 (Thermo Fisher Scientific, Massachusetts, USA) and anticaudalizing agents (Noggin (Thermo Fisher

Scientific, Massachusetts, USA), DKK1 (PeproTech, New Jersey, USA), Cyclopamine (Merck, Darmstadt, Germany), and SB431542 (Sigma, Missouri, USA)). The treatment was repeated every other day. On day 20 the EBs were moved to a poly-ornithine (Sigma, Missouri, USA)/laminin (Thermo Fisher Scientific, Massachusetts, USA) coated plate to support further differentiation in adherent conditions. On Day 27 or later, manually picked rosettes were dissociated by Accutase (Thermo Fisher Scientific, Massachusetts, USA) and re-seeded onto a new poly-ornithine/laminin coated plate in DMEM/F-12, GlutaMAX™ N2/B27 medium containing FGF2 (Thermo Fisher Scientific, Massachusetts, USA) and laminin. The attached neural progenitor cells (NPCs) showed uniform morphology after 5 passages. The NPCs between passage p5 and p15 were used for the experiments. For neuronal differentiation experiments NPCs were further differentiated NPCs were seeded onto poly-ornithine/laminin coated, in eight-well Nunc Lab-Tek II Chambered Coverglass (Nalgene Nunc International, New York, USA) with 1.5x103 density in N2/B27 medium supplemented with ascorbic acid (Sigma, Missouri, USA), BDNF (PeproTech, New Jersey, USA), cAMP (Sigma, Missouri, USA), Laminin and Wnt3A (Research and Diagnostic Systems Inc, Minnesota, USA). After 3 weeks Wnt3A was omitted from the medium. The medium was changed every other day.

### Molecular characterization of neuronal progenitors and neurons

For immunofluorescence staining of NPCs and NPC-derived neurons from the case-parent trio and the unrelated control cell line, NPCs were seeded onto poly-ornithine/laminin coated, eight-well chambers, and differentiated into DG neurons for 5 weeks as described above. The cells were fixed with 4% paraformaldehyde (Thermo Fisher Scientific, Waltham, Massachusetts, USA) in Dulbecco's modified PBS (DPBS) (Sigma, Missouri, USA) for 15 min at room temperature. Following washing with DPBS, the samples were blocked for 1h at room temperature in DPBS containing 2 mg/ml bovine serum albumin (Sigma, Missouri, USA), 1% fish gelatin (Sigma, Missouri, USA), 5% goat serum (Sigma, Missouri, USA) and 0.1% Triton-X 100 (Sigma, Missouri, USA). The samples were then incubated for

1h at room temperature with the following antibodies: anti-SOX2 (monoclonal/mouse, 1:20 dilution; MAB2018, R&D Systems, Minneapolis, USA), anti-Nestin (polyclonal/rabbit, 1:250 dilution; ab92391, Abcam, Cambridge, UK) or for overnight at 4oC with the following antibodies: anti-PROX1 (polyclonal/rabbit, 1:500 dilution; ab101851, Abcam, Cambridge, UK), anti-MAP2 (monoclonal/mouse, 1:500 dilution; M1406, Sigma/Merck, Darmstadt, Germany or polyclonal/rabbit, 1:1000 dilution; ab5622, Millipore, Massachusetts, USA). The proteins encoded by the genes of interest harboring DNMs were also investigated by immunofluorescence staining, using anti-KHSRP (1:1000 ab140648, Abcam, Cambridge, UK) and anti-LRRC7 (1:500, HPA005625, Sigma/Merck, Darmstadt, Germany) antibodies. After washing with DPBS, the cells were incubated for 1h at room temperature with appropriate secondary antibodies; Alexa Fluor 633-conjugated goat anti-mouse IgG or Alexa Fluor 547-conjugated goat anti-rabbit IgG (Thermo Fisher Scientific, Massachusetts, USA). The nuclei were counterstained with DAPI (Thermo Fisher Scientific, Massachusetts, USA). The stained samples were examined by a Zeiss LSM 900 confocal laser scanning microscope. Fluorescence images were analyzed with the ZEN 3.1 blue edition software. In the confocal images pseudo-color coding was used for better visualization.

## Gene expression analysis

Total RNA was isolated from NPCs and NPC-derived neurons using TRIzol™ reagent following the manufacturer’s instructions (Thermo Fisher Scientific, Massachusetts, USA). cDNA samples were prepared from 0.2 µg total RNA using the Promega Reverse Transcription System Kit (Promega, Wisconsin, USA) as specified by the manufacturer. For real-time quantitative PCR the following Pre-Developed TaqMan® assays were purchased from Thermo Fisher Scientific, Massachusetts, USA: NANOG as undifferentiated stem cell marker; Pax6 , and SOX2 as markers of NPC state, as well as NeuroD1, FoxG1, and PROX1, GRIA1 as neuronal differentiation specific markers; P0 ribosomal protein as endogenous control for quantification. KHSRP and LRRC7 expression were examined as well. RT-PCR analyses were carried out using the StepOnePlus™ Real-Time PCR System

(Thermo Fisher Scientific, Massachusetts, USA), according to the manufacturer's instructions. The changes in mRNA levels between the examined and control cells were determined by the 2-ΔCt method using RPLP0 (P0) as endogenous control gene. Relative mRNA levels were presented as heatmaps using the mean values of 3 independent experiments.

## RNA-Sequencing experiments

RNASeq experiments were carried out at the NPC stage for each cell line in quadruplicates. RNA was isolated at 4 different passages from each NPC line between p7-12 to ensure biological replicates. After library preparation samples were sequenced with the Illumina HiSeq technology using 2x150 bp paired-end reads resulting in 40 million read-pairs (12 Gb sequence) coverage per sample.

Mapping to the Homo sapiens (hg19) reference genome was performed using Hisat2 software, after quality control of raw reads with FASTQC and trimming with Trimgalore. Mapped reads were annotated to genes using featureCounts function of the Subread R package. All X and Y chromosome genes were excluded from downstream analyses. To compare transcriptomic differences we performed differential gene expression (DE) analysis, principal component analysis, and cluster analysis using the DESeq2 R package, PCAExplorer, Cluster 3.0, and Treeview, respectively. Differentially expressed genes between two NPC lines were selected if the logarithmic of fold change was greater than 1 and adjusted p-value smaller than 0.1.  Gene Ontology (GO) and Pathway analysis of DE genes were performed using DAVID. DE genes were significantly enriched in GO and PATHWAY terms when their FDR was less than 0.1.

## $Ca^{2+}$ signal measurements in NPC cultures

Before the $Ca^{2+}$ measurements NPCs were seeded for two days onto eight-well chambers previously coated with poly-ornithine/laminin. NPCs cells were subjected to 1.0 µM Fluo-4 AM (Thermo Fisher Scientific, Massachusetts, USA) in a serum free culture medium for 30 min at 37°C. Extracellular Fluo-4 AM was removed by changing the medium to Hanks' balanced salt solution (Thermo Fisher Scientific, Massachusetts, USA) supplemented with 20 mM Hepes (pH=7.4) (Thermo Fisher Scientific, Massachusetts, USA) and 0.9 mM $MgCl_2$ (Sigma, Missouri, USA) (HBSS). All measurements were performed in HBSS at room temperature. The ligand concentrations were chosen according to literature: glutamate (50 µM) (Sigma, Missouri, USA), KCl (50 mM) and ionomycin (5 µM) (Thermo Fisher Scientific, Massachusetts, USA). All experiments were performed at room temperature.

$Ca^{2+}$ signal measurements were carried out by acquisition of time lapse sequences of fluorescence images with an Olympus laser scanning confocal microscope and using the FluoViewTiempo (v4.3, Olympus, http://www.olympusmicro.com) software as described earlier (29). Fluorescence images were acquired between 505 and 525 nm at 488 nm excitation. Image analysis was carried out with the same software. The cellular fluorescence signals measured in regions of interest (ROIs) placed over the cells were converted to percentage of activation based on (F-Fmin)/(Fmax-Fmin) *100, where F is the $Ca^{2+}$ signal intensity at a given time point, Fmin is the minimum of the first fifteen time points and Fmax is the maximum after the administration of ionomycin. For further analysis we used those cells, which reached at least 10% activity after glutamate administration. We used Chi-square statistics to compare the percentage of activated cells between subjects. Furthermore, in activated cells we derived F/F0, where F0 is the minimum of baseline activity before glutamate administration (5 time points), and F is the maximum $Ca^{2+}$ signal intensity of 50 time points after glutamate administration. Data are means (±SD) of all the individual cells (typically 150-250 cells for each subject and each parallel experiment). For statistical comparison between subjects (mother, father and patients with schizophrenia) we conducted ANOVA for the dependent variable (F/F0) and

used the 3 parallel experiments as covariates. Statistical analysis was conducted with the SPSS software.

## Functional phenotyping of NPC lines (cell proliferation, neuronal migration, neurite outgrowth)

Based on the RNASeq results, we performed targeted functional assessment of NPCs, namely cell proliferation, neuronal migration, and neurite outgrowth tests. For the 96-hour proliferation assays, 35.000 NPCs were plated per well in a 24-well plate using triplicates for each time point. NPCs were harvested and labeled with the viability marker propidium iodide then measured in a total volume of 120 µl by Attune flow cytometry at 24 and 48 hours after. For assessment of NPC migration, we used the scratch or „wound healing" test, as described earlier (30). 450.000 NPCs were seeded onto poly-ornithine/laminin coated, six-well plates. After reaching confluence scars were inflicted manually in each well in triplicates. NPC migration was measured at 24 and 48 hours on bright field micrographs. For neurite outgrowth experiments we used NPCs treated with calcein (10mM). 3.500 NPC-s were seeded per well in 96-well plates, after 2 hours the cells were treated with para-nitroblebbistatin (10mM), a known inductor of neurite outgrowth (31) or DMSO. Neurite outgrowth was visualized and measured by fluorescence microscopy using the automated image acquisition and analysis system of the ImageXpress High content screening system. Data were evaluated and significance levels determined using the GraphPad Prism 8.3.0 software.

## Oxidative stress and mitochondrial tests

Oxidative stress tolerance was investigated in NPC lines by treatment with $CoCl_2$, a well-known hypoxia inducer and reoxygenation (32). Cell lines were plated at a number of 35.000 cells/well in poly-ornithine/laminin coated 48-well plates using triplicates. Medium

was replaced after reaching confluence with $CoCl_2$ containing media at two different concentrations (control=0µM, 125µM, 250 µM). After 24 hours, the medium was changed to normal medium (reoxygenation). Two days after reoxygenation, viability was measured using the PrestoBlue dye and the fluorescent signal intensity was measured by Enspire Multimode plate reader (Perkin Elmer). NPCs were characterized by their baseline levels of reactive oxygen species (ROS) using the CellROX kit (Thermo Fischer Scientific, Cat. Number: C10444). NPCs were dissociated by accutase and then 200.000 cells were incubated/treated with CellROX at 500x dilution for 30 minutes at 37°C. After the incubation period cells were washed three times with 1x PBS. Subsequently, the mean fluorescence signal of labeled cells was measured and compared by flow cytometry (Attune NxT Flow Cytometer, ThermoFisher), and the dead cells were gated out by using propidium iodide staining.

Mitochondrial function in NPCs was examined by Mitotracker staining and transmission electron microscopy. The Mitotracker Red dye (MitoTracker ™ Red CMXRos, cat. Number: M7512) was applied on NPC cultures after reaching confluence at a concentration of 250 nM. After 30 min incubation at 37°C the dye was washed with DPBS, and the NPCs were fixed by 4% PFA for 15 minutes at RT. Fluorescent signals were acquired by confocal microscopy (Zeiss LSM 900). Images were evaluated with the NIH Image J software by comparing total fluorescence intensity per nucleus. For transmission electron microscopy, briefly, NPCs were dissociated manually or enzymatically with Accutase, the samples were fixed with solution containing 3.2% PFA, 0.2% glutaraldehyde, 1% sucrose, 40mM $CaCl_2$ in 0.1M cacodylate buffer. Next, samples were post-fixed with 1% ferrocyanide-reduced osmium tetroxide and dehydrated using a graded ethanol series, and then embedded in Spurr low viscosity epoxy resin medium. Ultrathin sections were collected on Formvar (Agar Sci., Essex, UK) coated copper slot grids, counterstained with uranyl acetate and Reynolds's lead citrate, and examined on a JEOL JEM 1011 transmission electron microscope equipped with a Morada 11-megapixel camera (Olympus) using iTEM software.

### Statistical analysis

All experiments were carried out in triplicates. Values are presented as mean ± SD for all experimental data. Comparisons between groups were performed by using one-way ANOVA followed by Dunn's post hoc testing. Outliers were removed by Grubb's test. The P-value $< 0.05$ was considered to indicate a significant difference. If otherwise not indicated, statistical analyses and curve-fitting were performed in GraphPad Prism 8.3.0 software.

## Results

### iPSC generation, NPC differentiation, molecular characterization

We successfully reprogrammed PBMCs into iPSCs for subsequent differentiation experiments. All iPSC lines demonstrated typical morphological properties, expressed pluripotency markers, were devoid of karyotype abnormalities (Figure 1c,d and Supplementary figure 1a-c). The previously described DNMs were also back-validated in iPSCs using Sanger sequencing (Figure 1e). The iPSCs had low levels of spontaneous differentiation in pluripotency conditions, but were able to differentiate into all 3 germline layers, as revealed by spontaneous differentiation experiments (Supplementary Figure 1d). The NPC lines generated form the case-parent trio and an unrelated healthy control subject (Figure 2a) demonstrated uniform molecular and morphological properties as captured by gene expression analysis (Figure 2b) and immunofluorescence microscopy (Figure 2c), respectively. We observed no differences in the NPC lines' efficiency to differentiate into neurons. The morphological properties and functional maturity of these neurons were tested by immunofluorescence staining (Figure 2d), Ca-imaging and single-cell patch-clamp recordings (results not shown), respectively. We included DNM harboring target genes KHSRP and LRRC7 in our molecular assays to test for potential differences at the RNA or protein expression levels, but found no significant differences (Figure 2b and e,f).

### RNASeq analyses

Next, to investigate whole-genome transcriptomic differences at the neuronal progenitor state that might be associated with the DNMs carried by the proband, or his disease status we carried out RNA sequencing analyses. The RNASeq experiments and subsequent bioinformatics analyses demonstrated a clear separation of cell lines tested by principal component analysis and cluster-analysis (Figure 3a-b). We identified a set of differentially expressed (DE) genes, that were down or upregulated in the SZ-HU-PROB NPC lines compared to both the paternal (SZ-HU-FA) and maternal (SZ-HU-MO) NPC lines (Figure 3c and Supplementary Tables 1 and 2). These gene-sets were taken forward for GO- and PATHWAY analyses (Figure 3d) that indicated the enrichment of DE genes in relevant biological pathways, including neuroactive ligand-receptor interaction, axon guidance, synapse, frizzled binding, enteric nervous system

development. Among the 100 top up- and downregulated genes were several transcription factor and neuron-specific genes.

Based on the known biological functions of KHSRP we tested for enrichment in the known targets of the KHSRP protein, namely GAP43, TNF, IL1A and B, ILR2B, FOS and all miRNAs. Out of these 5 protein-coding genes IL1A and ILR2B were downregulated, moreover we observed up-regulation of 5, and down-regulation of 5 miRNAs, compared to the other two cell lines.

## $Ca^{2+}$ imaging experiments

As transcriptomic differences were indicative of synaptic and $Ca^{2+}$ binding differences, moreover we wanted to test the functional activity of the progenitors, therefore, we used $Ca^{2+}$ imaging to investigate the spontaneous activity and glutamate-evoked reactivity of NPCs. Similarly to our previous results, NPCs demonstrated low levels of spontaneous activity but reacted to stimulation with glutamate (27). We found that among patient-derived NPCs the proportion of activated cells is significantly lower. In addition, these NPCs demonstrated a significantly dampened reaction to glutamate in the average of the 3 experiments. There were other significant differences between the other 3 healthy subjects in both measures (percentage of activated cells and F/F0 after glutamate administration in Figures 4a-d and Supplementary Figures 2a,b).

## Proliferation, migration, and neurite outgrowth tests in NPCs

Based on earlier results from iPSC-based experiments carried out by other groups and our transcriptomic findings, we also tested for potential differences in NPC proliferation and migration, furthermore neurite outgrowth speed of differentiating NPCs. The aggregate kinetics of proliferation, migration and differentiation have been shown earlier to determine the efficiency of neuronal differentiation in these progenitor populations. We found that NPC-s derived from the proband, consistently with the upregulation of several Wnt-species in these cells (Figure 3d and supplementary table 1), show increased cell proliferation compared to the maternal, paternal and healthy control NPCs (Figure 5a). These findings were underscored by faster migration in the same NPC-s, as measured by the scratch test, a functional assessment that measures both proliferation and migration kinetics (Figure 5b-c and Supplementary figure 2c,d). As a continuation of these experiments we investigated neurite outgrowth in differentiating NPC-s, either at baseline conditions, or by chemical stimulation of neurite outgrowth with para-nitroblebbistatin (PNBS), an established inductor of neurite outgrowth. At baseline conditions we observed accelerated neurite outgrowth in the proband-derived and paternal NPC lines compared to the unrelated control and maternal NPC lines, only in the control conditions. Treatment with PNBS abolished these differences (Figure 5d-e and Supplementary figure 2e).

### Assessment of mitochondrial function and tolerance to oxidative stress

We used two independent methods to test for alterations in reactive oxygen species and tolerance to oxidative stress, phenotypes reported earlier in schizophrenia-derived cell lines. Surprisingly, there were lower levels of ROS in the proband-derived NPC line, that were statistically not significant (Supplementary figure 2f), and no differences were found in the tolerance of cell lines to oxidative stress evoked by treatment with $CoCl_2$ for 24 hours and subsequent reoxygenation (Figure 6a-b and Supplementary figure 2g).

Next, for quantification of mitochondria in NPCs a mitochondrion-specific dye was used that allows measurement of functional mitochondria based on fluorescence intensity. This demonstrated significantly decreased quantity of functional mitochondria in NPC-SZ-HU-PROB in comparison to both the maternal cell line and the healthy control cell line (Figure 6c-d and Supplementary figure 2h). Finally, we used transmission electron microscopy to investigate the morphology of mitochondria in the trio NPC lines. This high-resolution method revealed abnormal, distensed, vacuolized and broken mitochondria with irregular structure of cristae compared to the elongated, regularly membranized, often fusioned mitochondria found in NPC lines SZ-HU-MO and SZ-HU-FA (Figure 6e, representative images).

## Discussion

Throughout our experiments we sought to investigate the biological significance of DNMs identified in a patient suffering from schizophrenia, using iPSCs and neuronal differentiation as a model system in a case-parent trio design. By the combination of several methodological approaches we were able to identify molecular and functional phenotypes demonstrating differences between cell lines that can be connected to neurodevelopmental pathology, and in part also to the investigated DNMs. The identified cell-autonomous phenotypes partially fall in line with previous iPSC-based disease modeling results of schizophrenia, however, some of the results are more typical for ASD. To our best knowledge this is the first study that has performed reprogramming in a whole trio to test for putative molecular disease pathways in schizophrenia. Similar studies can pave the way in the future for a personalized, precision medicine-based approach in the field of iPSC-based disease-modeling studies.

Consistent with previous findings all iPSC lines were capable of neuronal differentiation, resulting in homogeneous SOX2 and NESTIN-expressing neuronal progenitors, and subsequently, by further differentiation in MAP2 and PROX1-expressing, functional, dentate gyrus neurons. Interestingly, qPCR-analyses demonstrated a tendency for more efficient neuronal differentiation, as captured by higher expression of neuronal marker genes NeuroD1 and PROX1 in the proband-derived and paternal neuronal cultures. Yu et al. reported a dampened expression of neuronal markers in SZ-derived differentiating neurons (28), however in our trio we found nearly equal expression of these markers between the investigated cell lines. The mature neuronal cultures differentiated from the investigated NPC lines were

functional, demonstrated by spontaneous activity in Ca-imaging experiments and Na-currents measured by patch-clamp electrophysiology (results not shown). However, we performed no direct comparisons at the neuronal level, since the primary focus of the study was the neuronal progenitor stage.

Whole-genome transcriptome analysis allows for the investigation of more subtle, network-level differences between cell lines. The transcriptome-level alterations and the clear separation of samples from different individuals of the trio in the PCA and cluster-analysis serve as a proof-of-concept for the used trio-based approach. The lists of up- and down-regulated DE genes contain several candidate genes warranting further analysis. Among the upregulated DE genes, GSX1 is a transcription factor that plays an important role in the development of ventral telencephalon interneurons. Wnt3A, Wnt6 and Wnt10A both play an important role in brain and neuronal crest development. SCARA5, the most downregulated gene in the proband-derived NPCs is associated with suicidal behavior in a recently published genome-wide association study (33). Synapsin 3 (SYN3), another top downregulated DE gene, has been implicated in the regulation of hippocampal neurogenesis (34), and associated with schizophrenia in genetic studies (35). GO- and PATHWAY-analysis of up- and downregulated DE genes identified several enriched terms that are relevant for schizophrenia (neuroactive ligand-receptor interaction, axon guidance, synapse, frizzled binding), or for the involvement of KHSRP (transcriptional activator activity, RNA-binding). Of these, the most important finding is the involvement of Wnt-signaling that has been established in several genetic and disease-modeling studies in schizophrenia. We also observed misregulation of several miRNA-species, however caution should be taken regarding these findings, as the resolution of the sequencing was not optimized for small RNAs. An important limitation of the transcriptomic analyses in this study was the fact that we didn't use an external control, as in other experiments. Therefore, the identified differences are only based on comparisons between trio-members.

To test for functional differences between cell lines we performed $Ca^{2+}$ imaging experiments in NPC-cultures. Previous work has shown that NPCs are amenable to measurements of intracellular $Ca^{2+}$ signaling, which is reflective of the reactivity of neuronal progenitors to different ligands. Moreover, alterations have been shown both in schizophrenia and ASD disease modeling-studies (28). We tested the NPCs reactivity to glutamate, given the fact that dentate gyrus progenitors receive glutamatergic inputs. Although we showed that a proportion of NPCs react to glutamate in all cell lines, and in 2 out of 3 experiments the proportion of glutamate-reactive NPCs was lower in the proband-derived NPCs, overall we could not show specific functional differences using $Ca^{2+}$ imaging.

Several differences in proliferation, migration, neurite outgrowth, oxidative stress, and mitochondrial function could be identified between NPC lines. Several of these alterations were informed by either transcriptomic differences identified with RNASeq, or by previous findings of other groups. In particular, the increased rate of cell NPC proliferation and migration found in the proband-derived lines is consistent with the transcriptomic alterations in Wnt-signaling and cell-adhesion. Marchetto et al. demonstrated increased level of progenitor proliferation in idiopathic ASD-derived NPCs that was mediated by the upregulation of β-catenin signaling (36). Similarly in a cohort of idiopathic ASD-patients Schäfer et al. showed the temporal dysregulation of specific gene networks that leads to growth acceleration in the

patient-derived neuronal progenitors (37). Both accelerated and decreased neurite outgrowth have also been implicated as important neurodevelopmental cell-autonomous phenotypes in ASD and schizophrenia. In an IPSC-based model of Kleefstra-syndrome, a syndromic subtype of ASD, NPCs demonstrated increased proliferation, while neurite arborization was reduced in mature neurons (38). It has also been shown that KHSRP regulates the mRNA-stability of GAP43, an important player in the process of axonal and dendritic growth (39). Genetic manipulation of KHSRP manifested itself in altered axonal growth in mouse primary neuronal cultures. We were able to identify subtle difference in neurite outgrowth, with increased rates in the proband-derived and paternal progenitors. Both the increased NPC proliferation and accelerated neurite outgrowth are phenotypes that were previously associated with ASD, however in the investigated schizophrenia trio, they could also be identified. Grunwald et al. (40) used iPSC-based methodology to make head-to-head comparisons between schizophrenia and ASD-derived neural cells, and also found overlapping phenotype, but were able to discriminate schizophrenia and AD-derived neurons by the combination of transcriptome analysis and $Ca^{2+}$imaging.

Finally, we found no alteration in tolerance to oxidative stress, and surprisingly, nominally lower levels of spontaneous reactive oxygen species in the proband-derived NPC lines. However, there was a clear decrease in the number of functional mitochondria in the proband-derived NPCs, and electron microscopic images were suggestive of altered mitochondrial morphology in these cell lines. Mitochondrial pathology has been previously implicated in several neurodevelopmental and neurodegenerative disorders, including amyotrophic lateral sclerosis, Parkinson's disorder and Alzheimer's disorder, i.e. dementia. Several lines of evidence suggest the involvement of mitochondrial dysfunction in cellular models of schizophrenia. Robiscsek et al. described that mitochondrial respiration and its sensitivity to dopamine-induced inhibition were impaired both in patient-derived keratinocytes and iPSCs. In differentiating dopaminergic neurons they found altered mitochondrial network structure and connectivity (41). In another study examining schizophrenia-derived NPCs from 4 patients, both mitochondrial dysfunction, as captured by the JC-1 red/green fluorescent dye measuring mitochondrial membrane potential, and oxidative stress, assessed by an OxyBlot procedure that quantifies the level of ROS-induced oxidized proteins, were elevated in the schizophrenia-derived cell lines compared to healthy controls (42). In the same cohort immunohistochemical staining and TEM revealed altered mitochondrial pathology. In our NPCs, we found no differences in ROS, however mitochondrial pathology could be demonstrated.

## Limitations

Limitations of this study have to be discussed. It has been mentioned that there is a bipolar patient in the investigated family, who was not included in the experiments. Therefore it is highly probable that the schizophrenia patient, besides the identified DNMs, which are attributable to the disorder, also carries a considerable level of genetic liability conveyed by common variants. Genome editing, e.g. CRISPR, which

we didn't use in our experiments, would be the most appropriate method to investigate the specific effects of the DNMs, and connect the putative cellular phenotypes selectively to the DNMs.

Several studies connect LRRC7 function to neurodevelopmental pathology, including ASD, language impairment, and ADHD. In a recent LRRC7 KO animal model it was shown that mutant animals have higher levels of anxiety and adulthood social dysfunction, parallel with reduced dendritic complexity, and increased dendritic spine length. Thus it is possible that the ASD-specific alterations unraveled in the presented experiments are associated with the DNM harbored in LRRC7. However, contrary to the cited study, we show evidence for accelerated neurite outgrowth, moreover, the methodology applied in our experiments wasn't appropriate to selectively test the different DNMs carried by the patient, therefore we can't make any statements about the specific effects of the different DNMs found in the patient.

# Conclusions

Overall, using different methodological approaches we could demonstrate several phenotypes in a schizophrenia patient-derived NPC line. Many of these phenotypes, i.e. NPC proliferation, migration, and neurite outgrowth have been associated previously with both schizophrenia and ASD as well. According to our results, it is conceivable that there is a convergence of phenotypes between schizophrenia and ASD in disease-modeling studies. These two disorders, although clinically distinct, show considerable levels of overlap at the symptomatology and genetic levels. Therefore, it is plausible that we can detect overlapping phenotypes also in disease-modeling studies.

# List Of Abbreviations

CNV: copy number variant, DE: differentially expressed, DNM: de novo mutation, DPBS: Dulbecco's modified PBS, EB: embryoid body, GO: Gene Ontology, iPSC: induced pluripotent stem cell, KHSRP: K-homology type splicing regulatory protein, KIR2DL1: Killer cell immunoglobulin-like receptor 2DL1, KOS: hKlf4, hOct3/4, hSox2, LRRC7: Leucine Rich Repeat Containing 7 gene, MEF: mouse embryonic fibroblast, NPC: neuronal progenitor cell, PBMC: peripheral mononuclear cell, PNBS: para-nitroblebbistatin, ROS: reactive oxygen species, SNP: single nucleotide polymorphism, SNV: single nucleotide variant.

# Declarations


### Acknowledgements

The authors would like to thank Beáta Haraszti, Dóra Reé, Tünde Berecz, Kornélia Szebényi, András Füredi, Zoltán Hegyi, Gergő Vőfély, Katalin Szőcs, Kata Vincze, Judit Benkovits, Attila Pulay, Vivien Hársfalvi, Eszter Kiss, Irén Haltrich, András Málnási-Csizmadia, Krisztina Pesti and Árpád Mike for technical assistance and advice. The control iPSC line (62F) was kindly provided by Professor Fred H. Gage and Carol Marchetto (Salk Institute for Biological Studies, San Diego, California).

## Authors' contributions

EH participated in the conceptualization of the study, performed the cell culture experiments, gene expression analysis, immunofluorescence staining, and participated in the collection and analysis of data and writing of the manuscript. NV carried out the cellular oxidative stress tests and analyzed the data. ZE performed the proliferation assays and mitochondria staining and analyzed the data. ES, MB and CT participated in the $Ca^{2+}$ experiments and the collection, assembly and analysis of these data. BC conducted all bioinformatics analysis. BJ performed the electron microscopy experiments and analyzed these data. JK carried out the exome sequencing experiments and analyzed the data. LN and MMJ contributed to the administrative support and provision of study material and patients. LH and ZN took part in data analysis and interpretation, ÁA and JMR conceived the study, planned the methodology, coordinated the experiments, analyzed and interpreted the data, and wrote the manuscript. All authors read and approved the final manuscript.

## Funding

This study was funded by the National Research and Technology Office of Hungary (grant number NKTH SCHIZO-08 to LN and MMJ), the National Brain Research Program (NAP) of Hungary (grant numbers: KTIA_NAP_13-1-2013-0001 to LH, KTIA_NAP_13-2014-0011 to JR, and 2017-1.2.1-NKP-2017-00002 to ÁA, LH, JMR and MMJ). The research was also supported by the Higher Education Institutional Excellence Programme of the Ministry of Human Capacities in Hungary, within the framework of the Neurology thematic programme of Semmelweis University.

## Availability of data and materials

The RNASeq datasets generated during the current study are available at Gene Expression Omnibus (GEO) database (https://www.ncbi.nlm.nih.gov/geo/). All other data are available from the corresponding author on reasonable request.

## Ethics approval and consent to participate

The reprogramming and the study were approved by the Human Reproduction Committee of the Hungarian Health Science Council (ETT HRB). All participants gave written informed consent.

## Competing interests

The authors declare no competing financial interests.

# References


1. van Os J, Kapur S. Schizophrenia. Lancet. 2009;374(9690):635-45. Epub 2009/08/25.
2. Kahn RS, Keefe RS. Schizophrenia is a cognitive illness: time for a change in focus. JAMA psychiatry. 2013;70(10):1107-12. Epub 2013/08/09.
3. Hathy E, Kalman S, Apati A, Nemoda Z, Rethelyi JM. Modeling neurological and psychiatric disorders in vitro using induced pluripotent stem cells: highlighting findings in Alzheimer's disease and schizophrenia. Neuropsychopharmacologia Hungarica. 2016;18(4):188-98. Epub 2017/03/06.
4. Kalman S, Hathy E, Rethelyi JM. A Dishful of a Troubled Mind: Induced Pluripotent Stem Cells in Psychiatric Research. Stem cells international. 2016;2016:7909176. Epub 2016/02/04.
5. Wright R, Rethelyi JM, Gage FH. Enhancing induced pluripotent stem cell models of schizophrenia. JAMA psychiatry. 2014;71(3):334-5. Epub 2014/01/03.
6. Rethelyi JM, Benkovits J, Bitter I. Genes and environments in schizophrenia: The different pieces of a manifold puzzle. Neuroscience and biobehavioral reviews. 2013;37(10 Pt 1):2424-37. Epub 2013/05/01.
7. Psychiatric Genomics Consortium. Genome-wide association study identifies five new schizophrenia loci. Nature genetics. 2011;43(10):969-76. Epub 2011/09/20.
8. Psychiatric Genomics Consortium. Biological insights from 108 schizophrenia-associated genetic loci. Nature. 2014;511(7510):421-7. Epub 2014/07/25.
9. Ingason A, Rujescu D, Cichon S, Sigurdsson E, Sigmundsson T, Pietilainen OP, et al. Copy number variations of chromosome 16p13.1 region associated with schizophrenia. Molecular psychiatry. 2011;16(1):17-25. Epub 2009/09/30.
10. Stefansson H, Meyer-Lindenberg A, Steinberg S, Magnusdottir B, Morgen K, Arnarsdottir S, et al. CNVs conferring risk of autism or schizophrenia affect cognition in controls. Nature. 2014;505(7483):361-6. Epub 2013/12/20.
11. Purcell SM, Moran JL, Fromer M, Ruderfer D, Solovieff N, Roussos P, et al. A polygenic burden of rare disruptive mutations in schizophrenia. Nature. 2014;506(7487):185-90. Epub 2014/01/28.
12. Fromer M, Pocklington AJ, Kavanagh DH, Williams HJ, Dwyer S, Gormley P, et al. De novo mutations in schizophrenia implicate synaptic networks. Nature. 2014;506(7487):179-84. Epub 2014/01/28.
13. Yoon KJ, Nguyen HN, Ursini G, Zhang F, Kim NS, Wen Z, et al. Modeling a genetic risk for schizophrenia in iPSCs and mice reveals neural stem cell deficits associated with adherens junctions and polarity. Cell stem cell. 2014;15(1):79-91. Epub 2014/07/06.
14. Brennand KJ, Simone A, Jou J, Gelboin-Burkhart C, Tran N, Sangar S, et al. Modelling schizophrenia using human induced pluripotent stem cells. Nature. 2011;473(7346):221-5. Epub 2011/04/15.
15. Moslem M, Olive J, Falk A. Stem cell models of schizophrenia, what have we learned and what is the potential? Schizophrenia research. 2019;210:3-12. Epub 2018/12/28.

16. Wang M, Zhang L, Gage FH. Modeling neuropsychiatric disorders using human induced pluripotent stem cells. Protein & cell. 2019. Epub 2019/05/28.
17. Schrode N, Ho SM, Yamamuro K, Dobbyn A, Huckins L, Matos MR, et al. Synergistic effects of common schizophrenia risk variants. Nature genetics. 2019;51(10):1475-85. Epub 2019/09/25.
18. Rajarajan P, Flaherty E, Akbarian S, Brennand KJ. CRISPR-based functional evaluation of schizophrenia risk variants. Schizophrenia research. 2019. Epub 2019/07/07.
19. Lewis EMA, Meganathan K, Baldridge D, Gontarz P, Zhang B, Bonni A, et al. Cellular and molecular characterization of multiplex autism in human induced pluripotent stem cell-derived neurons. bioRxiv. 2019:620807.
20. Briata P, Bordo D, Puppo M, Gorlero F, Rossi M, Perrone-Bizzozero N, et al. Diverse roles of the nucleic acid-binding protein KHSRP in cell differentiation and disease. Wiley interdisciplinary reviews RNA. 2016;7(2):227-40. Epub 2015/12/29.
21. Perrone-Bizzozero N. Neuropsychiatric Implications Of RNA-Binding Proteins HuD And KSRP Revealed By Genome-Wide Identification Of Their Targets. European Neuropsychopharmacology. 2019;29(Supplement3):S721.
22. de Jong S, Boks MP, Fuller TF, Strengman E, Janson E, de Kovel CG, et al. A gene co-expression network in whole blood of schizophrenia patients is independent of antipsychotic-use and enriched for brain-expressed genes. PloS one. 2012;7(6):e39498. Epub 2012/07/05.
23. Chong CH, Li Q, Mak PHS, Ng CCP, Leung EHW, Tan VH, et al. Lrrc7 mutant mice model developmental emotional dysregulation that can be alleviated by mGluR5 allosteric modulation. Translational psychiatry. 2019;9(1):244. Epub 2019/10/05.
24. Boyington JC, Sun PD. A structural perspective on MHC class I recognition by killer cell immunoglobulin-like receptors. Molecular immunology. 2002;38(14):1007-21. Epub 2002/04/17.
25. ClinVar Database [database on the Internet]. [cited Januar 7th 2020]. Available from: https://www.ncbi.nlm.nih.gov/clinvar/.
26. Erdei Z, Lorincz R, Szebenyi K, Pentek A, Varga N, Liko I, et al. Expression pattern of the human ABC transporters in pluripotent embryonic stem cells and in their derivatives. Cytometry Part B, Clinical cytometry. 2014;86(5):299-310. Epub 2014/04/15.
27. Vofely G, Berecz T, Szabo E, Szebenyi K, Hathy E, Orban TI, et al. Characterization of calcium signals in human induced pluripotent stem cell-derived dentate gyrus neuronal progenitors and mature neurons, stably expressing an advanced calcium indicator protein. Molecular and cellular neurosciences. 2018;88:222-30. Epub 2018/02/10.
28. Yu DX, Di Giorgio FP, Yao J, Marchetto MC, Brennand K, Wright R, et al. Modeling hippocampal neurogenesis using human pluripotent stem cells. Stem cell reports. 2014;2(3):295-310. Epub 2014/03/29.
29. Pentek A, Paszty K, Apati A. Analysis of Intracellular Calcium Signaling in Human Embryonic Stem Cells. Methods Mol Biol. 2016;1307:141-7. Epub 2014/02/01.

30. Liang CC, Park AY, Guan JL. In vitro scratch assay: a convenient and inexpensive method for analysis of cell migration in vitro. Nature protocols. 2007;2(2):329-33. Epub 2007/04/05.
31. Rauscher AA, Gyimesi M, Kovacs M, Malnasi-Csizmadia A. Targeting Myosin by Blebbistatin Derivatives: Optimization and Pharmacological Potential. Trends in biochemical sciences. 2018;43(9):700-13. Epub 2018/07/31.
32. Munoz-Sanchez J, Chanez-Cardenas ME. The use of cobalt chloride as a chemical hypoxia model. Journal of applied toxicology : JAT. 2019;39(4):556-70. Epub 2018/11/30.
33. Gonzalez-Castro TB, Martinez-Magana JJ, Tovilla-Zarate CA, Juarez-Rojop IE, Sarmiento E, Genis-Mendoza AD, et al. Gene-level genome-wide association analysis of suicide attempt, a preliminary study in a psychiatric Mexican population. Molecular genetics & genomic medicine. 2019;7(12):e983. Epub 2019/10/04.
34. Kao HT, Li P, Chao HM, Janoschka S, Pham K, Feng J, et al. Early involvement of synapsin III in neural progenitor cell development in the adult hippocampus. The Journal of comparative neurology. 2008;507(6):1860-70. Epub 2008/02/14.
35. Porton B, Wetsel WC, Kao HT. Synapsin III: role in neuronal plasticity and disease. Seminars in cell & developmental biology. 2011;22(4):416-24. Epub 2011/08/11.
36. Marchetto MC, Belinson H, Tian Y, Freitas BC, Fu C, Vadodaria K, et al. Altered proliferation and networks in neural cells derived from idiopathic autistic individuals. Molecular psychiatry. 2017;22(6):820-35. Epub 2016/07/06.
37. Schafer ST, Paquola ACM, Stern S, Gosselin D, Ku M, Pena M, et al. Pathological priming causes developmental gene network heterochronicity in autistic subject-derived neurons. Nature neuroscience. 2019;22(2):243-55. Epub 2019/01/09.
38. Nagy J, Kobolak J, Berzsenyi S, Abraham Z, Avci HX, Bock I, et al. Altered neurite morphology and cholinergic function of induced pluripotent stem cell-derived neurons from a patient with Kleefstra syndrome and autism. Translational psychiatry. 2017;7(7):e1179. Epub 2017/07/26.
39. Bird CW, Gardiner AS, Bolognani F, Tanner DC, Chen CY, Lin WJ, et al. KSRP modulation of GAP-43 mRNA stability restricts axonal outgrowth in embryonic hippocampal neurons. PloS one. 2013;8(11):e79255. Epub 2013/11/19.
40. Grunwald LM, Stock R, Haag K, Buckenmaier S, Eberle MC, Wildgruber D, et al. Comparative characterization of human induced pluripotent stem cells (hiPSC) derived from patients with schizophrenia and autism. Translational psychiatry. 2019;9(1):179. Epub 2019/07/31.
41. Robicsek O, Karry R, Petit I, Salman-Kesner N, Muller FJ, Klein E, et al. Abnormal neuronal differentiation and mitochondrial dysfunction in hair follicle-derived induced pluripotent stem cells of schizophrenia patients. Molecular psychiatry. 2013;18(10):1067-76. Epub 2013/06/05.
42. Brennand K, Savas JN, Kim Y, Tran N, Simone A, Hashimoto-Torii K, et al. Phenotypic differences in hiPSC NPCs derived from patients with schizophrenia. Molecular psychiatry. 2015;20(3):361-8. Epub 2014/04/02.

# Figures

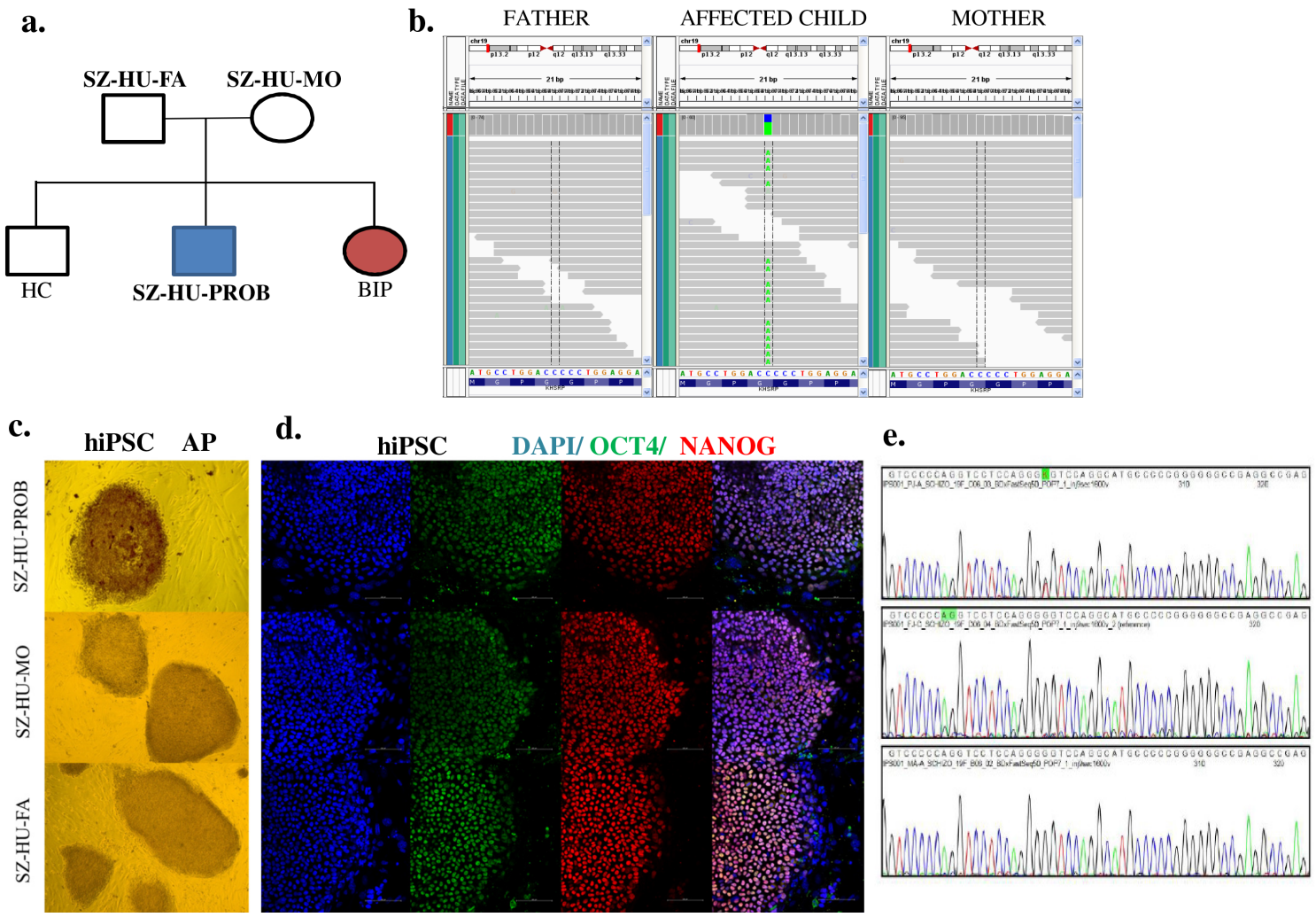


**Figure 1**

Selection of a schizophrenia case-parent trio based on ExomeSeq analysis and identified de novo mutations (LRRC7, KHSRP, KIR2DL1). Reprograming, characterization and quality control of iPSC lines. a Family pedigree of the investigated schizophrenia patient. b Representative diagram of a validated DNM in the trio visualized by Integrative Genomics Viewer c Alkaline phosphatase (AP) staining of hiPSCs. d Immunofluorescence staining for pluripotency markers; Oct4 (green) and Nanog (red) in hiPSCs. The high AP activity and positive staining for pluripotency markers confirmed pluripotent state of the generated iPSC lines. e Sanger sequence electropherogram of the stable iPSC lines. Results of Sanger sequencing proved that the germline DNMs (in LRRC7 and KHSRP genes) were preserved in the proband iPSC.

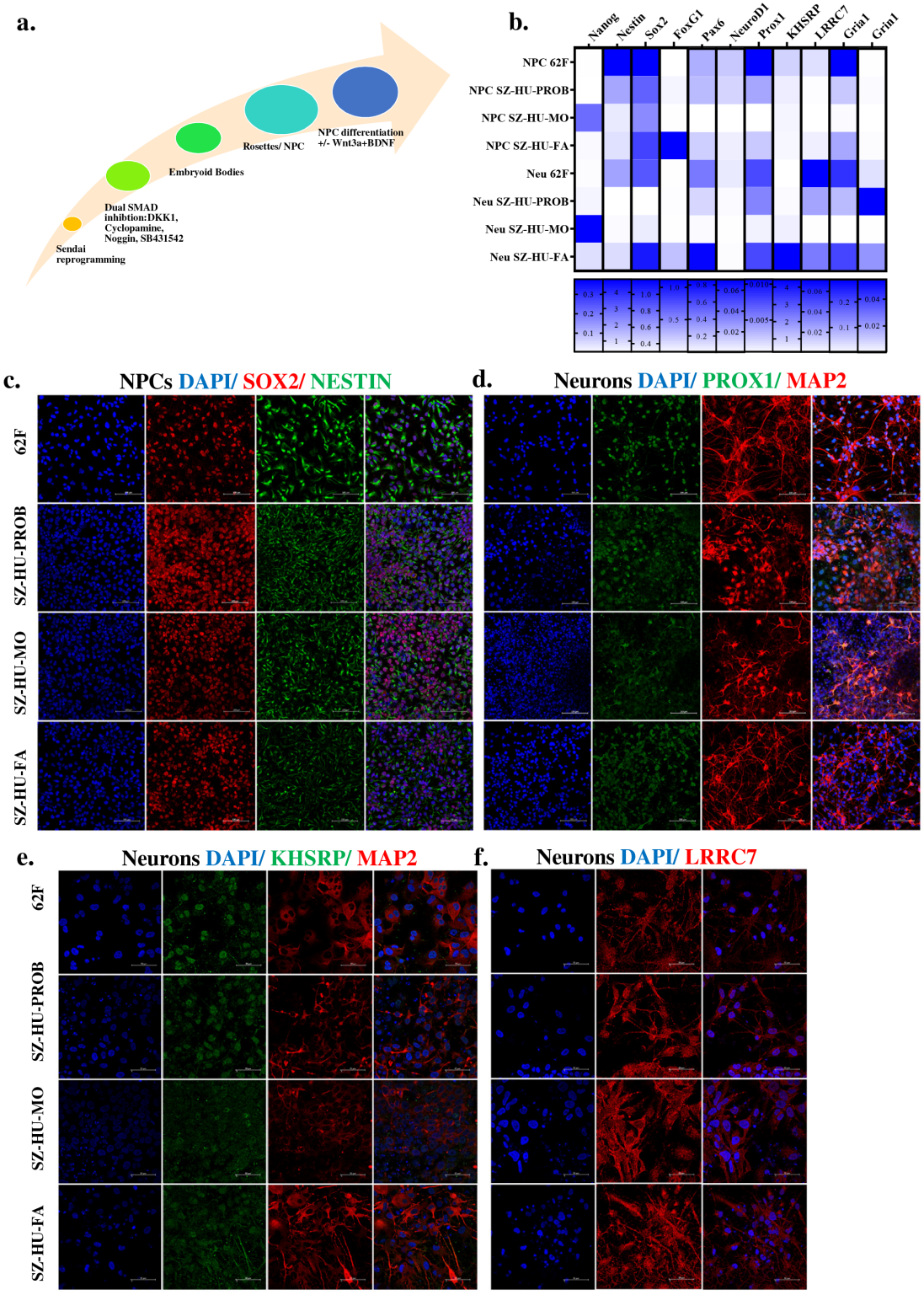


## Figure 2

Establishment and molecular characterization of NPC lines and mature neuronal cultures. Investigation of target genes KHSRP and LRRC7. a Schematic diagram of hippocampal neuronal differentiation. hiPSCs were differentiated as EBs in the presence of SMAD inhibitors Noggin and SB431542, the anticaudalizing Wnt antagonist Dkk1 or XAV939, and the SHH antagonist cyclopamine. After plating and rosette formation, neural progenitors (NPCs) are dissociated and expanded or further differentiated into

hippocampal dentate gyrus granule neurons in the presence of Wnt3A, BDNF, cAMP and ascorbic acid (AA). b Figure shows changes in gene expression patterns at NPCs and neurons derived from the case-parent trio. c-d NPCs and neurons derived from hiPSCs by the hippocampal neuronal differentiation protocol were investigated by immunofluorescence staining and visualized by confocal fluorescent microscopy. Immunocytochemical staining shows Nestin/Sox2 (c) and Map2/Prox1 (d) positivity in these established neural cell types. e-f Immunofluorescence staining for KHSRP and LRRC7 in neurons. KHSRP (e) shows nuclear and cytoplasmic localization, while LRRC7 (f) shows postsynaptic localization in neurons.

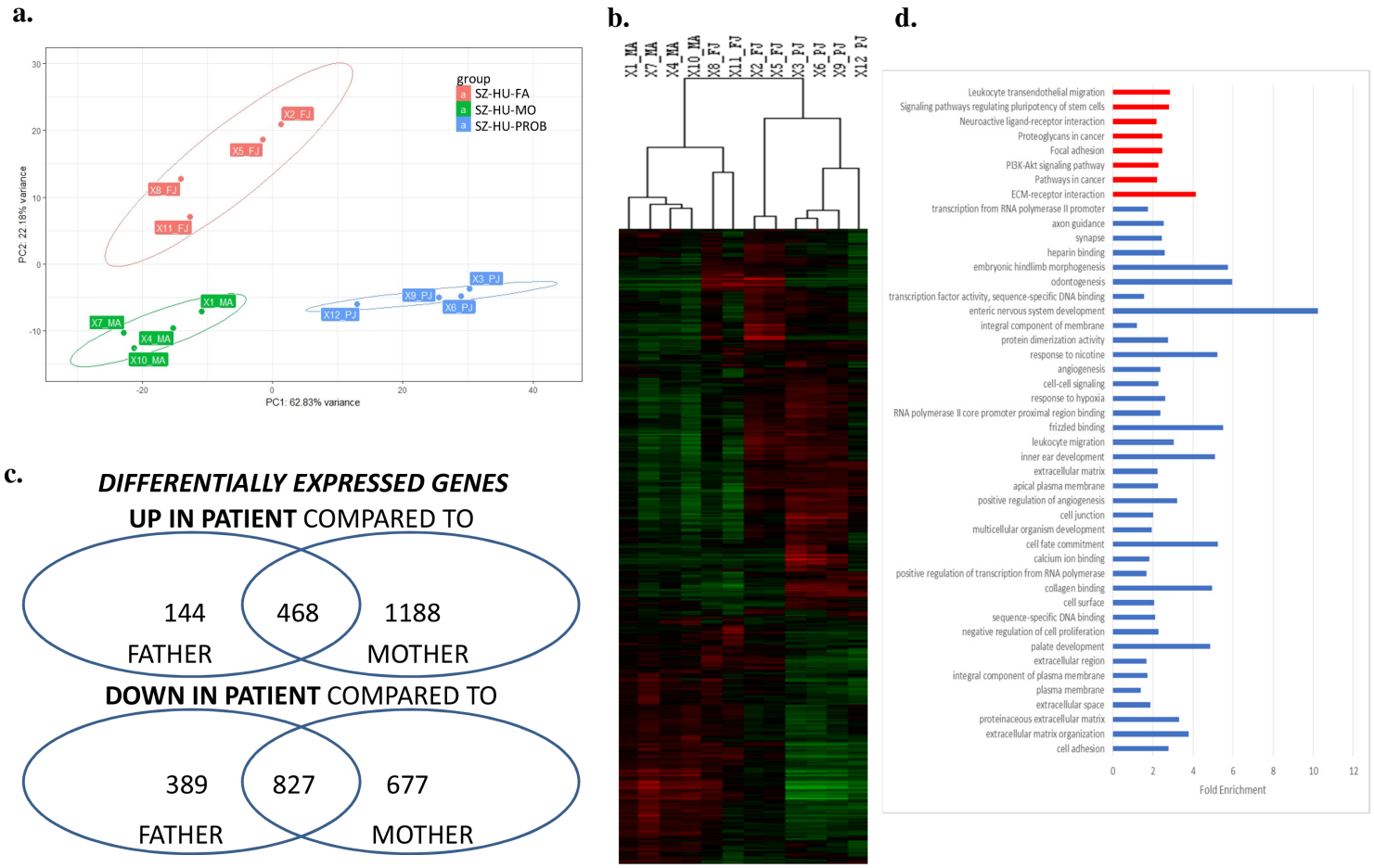


## Figure 3

Assessment of transcriptomic differences in the trio NPC lines using RNASeq. a-b Principal component and cluster analysis of gene expression values demonstrates a clear separation of RNASeq samples from different memebers of the trio. c Differential gene expression analysis identified significantly up- and downregulated genes. d Significantly enriched GO (blue) and PATHWAY (red) terms and fold enrichment values.

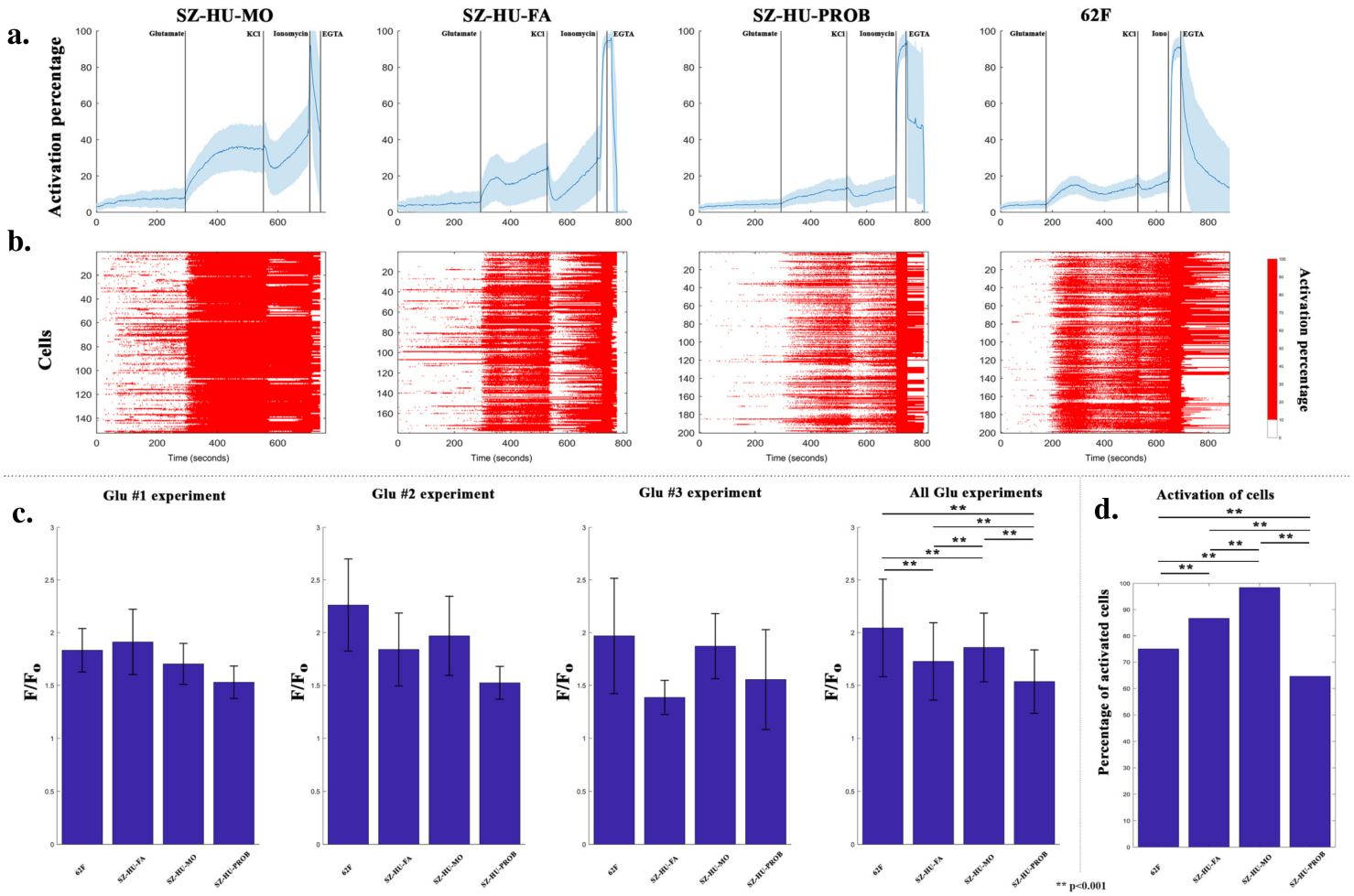


## Figure 4

Investigation of calcium-activity in NPCs. a-b The figure depicts the mean activation percentage of neuroprogenitor cells. Activity percentage (F percentage) was derived with (F-Fmin)/(Fmax-Fmin)*100 formula, where F is the Ca2+ signal intensity at a given time point, Fmin is the minimum of the first fifteen time points and Fmax is the maximum after the administration of ionomycin. We illustrated a representative experiment for the 4 subjects (a). The x axis represents the time (in seconds), at the top the y axis represents the activation percentage, and at the bottom the y axis represents the number of NPCs. The color represents the activity (white below 10% and red above 10%) (b). c The figure shows the mean and standard deviation of F/F0 for all subjects in the three parallel experiments and average of all experiments. Significant differences indicated with asterisks. The y axis represents F/F0, where F is the maximum Ca intensity of 10 time points after glutamate administration and F0 is the minimum of baseline activity before glutamate administration (5 time points). d The figure represents the average percentage of activated cells (compared to all cells) in the 3 experiments for all subjects. Significant differences indicated with asterisks.

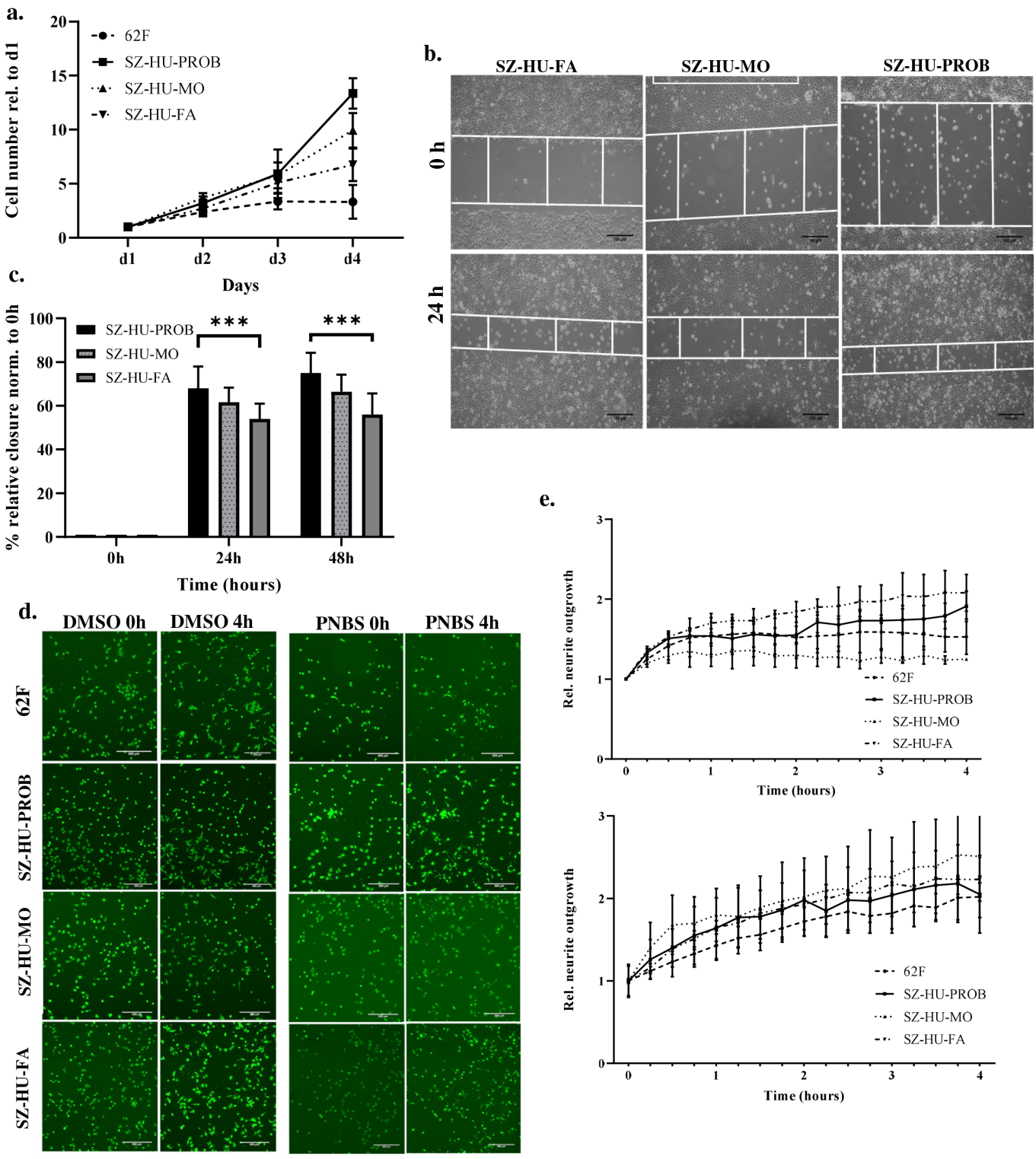


## Figure 5

Proliferation, neuronal migration and neurite outgrowth in the trio NPC-lines a Cell proliferation assay of NPCs. 35.000 NPCs were plated onto poly-ornithine/laminin coated plates and were further cultured for 4 days. Cells were harvested daily and cell number was measured by ATTUNE NXT flow cytometer. Non-viable cells were excluded by PI staining. The diagram shows the mean values of 3 independent experiments, each are performed with three technical parallels. b Representative images of scratch assay

on hiPSC-derived NPCs. For comparison of the migration and proliferation of control and patient-derived NPCs, equal numbers of NPCs were seeded onto each dish. Cells were cultured until confluency. Three parallel scratches were made per dish by a sterile P5 pipet. Three photos were taken along every scratches, at 24 and 48 hours. Manual analysis was performed using ImageJ. The rate of closure was defined by measuring the width of the two side of scratches. c Analysis of the scratch closure relative to day 0. The diagram shows mean values of two independent experiments, each with three replicate scratches, and three measurements per scratch. Data show the % of scratch closure normalized to 0h distance d, e Representative images of neurite outgrowth assay. NPCs were treated with para-nitroblebbistatin (PNBS) (10 μM). The changes of neurite outgrowth were monitored by high content screening which allowed the use of masking techniques to separate the cell body and outgrowths for further quantification. (d) Relative extent of neurite outgrowth. Diagrams show the neurite outgrowth of NPCs visualized by Calcein after 4h, normalized to 0h. Graph above: untreated cells (DMSO), graph below: treated cells (PNBS) (e).

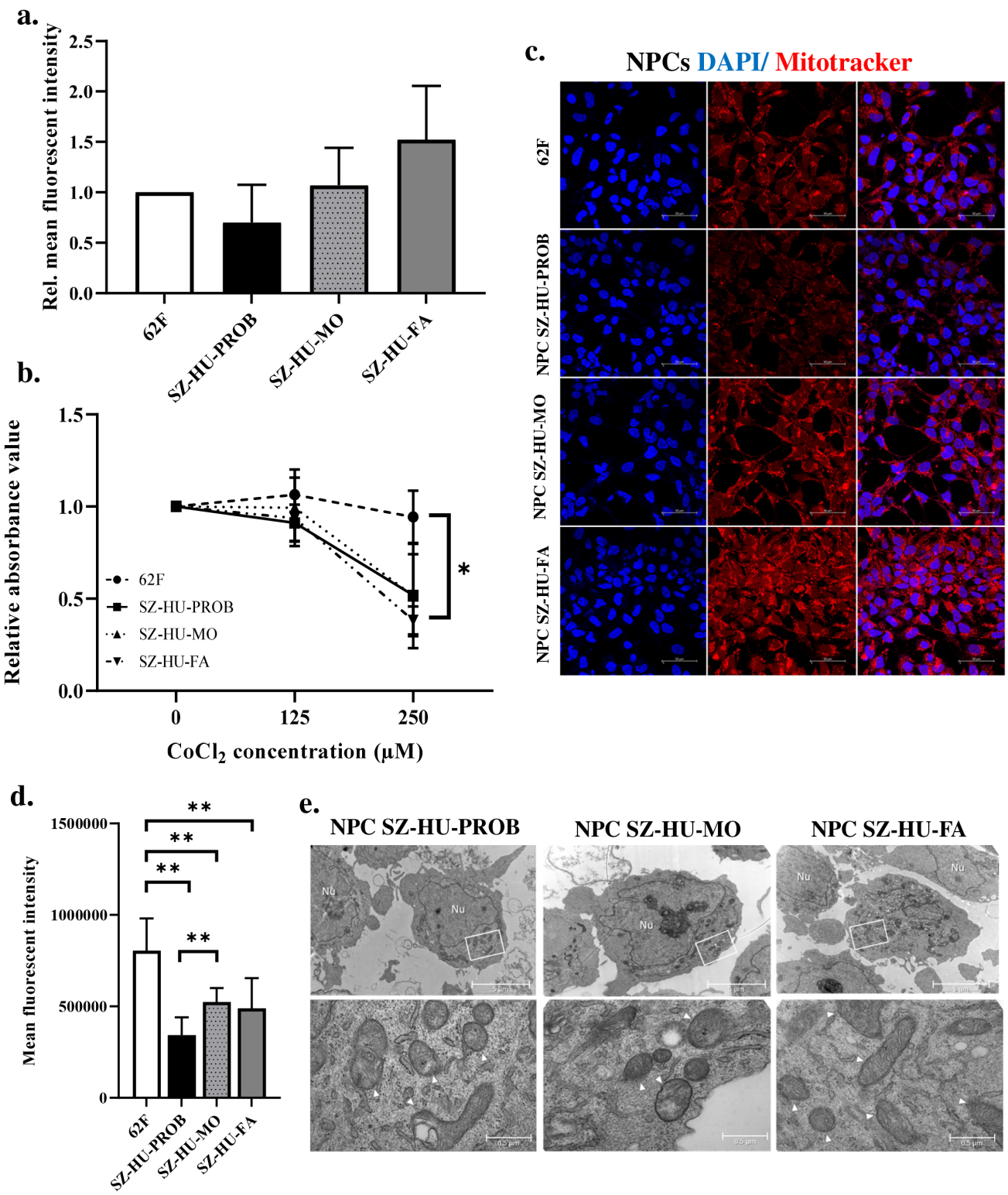


## Figure 6

Assessment of mitochondrial function and tolerance to oxidative stress in the trio NPC lines. a Quantification of reactive oxygen species (ROS) in NPCs using CellROX reagent. Diagram shows the mean fluorescent intensity of fixed and stained NPC lines, normalized to 62F (ctrl cell line). Fluorescent signal data were generated by quantification of confocal microscopy images (magnification: 40x). Analysis were performed using ImageJ. b Effect of CoCl2 treatment on NPC cell survival. NPCs were

treated with 125 and 250 μM CoCl2 for 24h. After 48h of reoxygenation, cell viability were measured by Presto Blue staining to determine the effect of oxidative stress. The fluorescent signal intensity was analyzed by Enspire Multimode plate reader. Values are normalized to untreated cells. The diagram shows the mean values of 5 independent experiments, each are performed with three technical parallels. c-e Examination of mitochondrial function in NPCs. Representative confocal microscopy images of NPC lines. Cells were stained using a fluorescent dye (MitoTracker) that stains the mitochondria in fixed cells (c). Quantification of MitoTracker staining. Diagram shows the mean fluorescent intensities of NPC cell lines. Data were generated from confocal microscopy staining with ImageJ (d). Mitochondrial morphology of mechanically dissociated NPC lines. Representative electron microscopy images of ultrathin sections (e).

## Supplementary Files

This is a list of supplementary files associated with this preprint. Click to download.

- DEGENESDOWNREG0102.docx
- DEGENESUPREG0102.docx
- supplfigureslegends.pdf